JACS
JOURNAL OF THE AMERICAN CHEMICAL SOCIETY
Communication
pubs.acs.org/JACS

Monodisperse Core/Shell Ni/FePt Nanoparticles and Their Conversion to Ni/Pt to Catalyze Oxygen Reduction

Sen Zhang,[†] Yizhou Hao,[‡] Dong Su,[§] Vicky V. T. Doan-Nguyen,[‡] Yaoting Wu,[†] Jing Li,[§] Shouheng Sun,[∥] and Christopher B. Murray*[,†,‡]

[†]Department of Chemistry and [‡]Department of Materials Science and Engineering, University of Pennsylvania, Philadelphia, Pennsylvania 19104, United States

[§]Center for Functional Nanomaterials, Brookhaven National Laboratory, Upton, New York 11973, United States

[∥]Department of Chemistry, Brown University, Providence, Rhode Island 02912, United States

Supporting Information

ABSTRACT: We report a size-controllable synthesis of monodisperse core/shell Ni/FePt nanoparticles (NPs) via a seed-mediated growth and their subsequent conversion to Ni/Pt NPs. Preventing surface oxidation of the Ni seeds is essential for the growth of uniform FePt shells. These Ni/FePt NPs have a thin (≈1 nm) FePt shell and can be converted to Ni/Pt by acetic acid wash to yield active catalysts for oxygen reduction reaction (ORR). Tuning the core size allows the optimization of their electrocatalytic activity. The specific activity and mass activity of 4.2/0.8 nm core/shell Ni/FePt after acetic acid wash reach 1.95 mA/cm^2 and 490 mA/mg$_{Pt}$ at 0.9 V (vs reversible hydrogen electrode), which are much higher than those of benchmark commercial Pt catalyst (0.34 mA/cm^2 and 92 mA/mg$_{Pt}$ at 0.9 V). Our studies provide a robust approach to monodisperse core/shell NPs with nonprecious metal core, making it possible to develop advanced NP catalysts with ultralow Pt content for ORR and many other heterogeneous reactions.

Precise control of Pt-based nanoparticle (NP) architecture at the atomic level has been demonstrated as an important approach to highly efficient catalysts for oxygen reduction reaction (ORR), a key cathodic reaction in polymer electrolyte membrane fuel cells and metal-air batteries.[1−6] This control over NP sizes,[7,8] shapes,[9−15] alloy compositions,[16−20] and intermetallic structures[21−25] has provided model catalysts for understanding the correlation of NP's architecture to the desired catalytic properties of high activity, durability, and selectivity. For example, alloying Pt with early transition metals, such as Ni, Co, Fe, can down-shift the d-band center of Pt, producing catalytic surfaces which weakly bind oxygenated intermediates, resulting in higher ORR activity.[17,26] Furthermore, by tailoring the Pt alloy/intermetallic NPs' shapes and compositions, their ORR efficiency can be enhanced by surface geometric and strain effects.[13,19,27] Despite these advances in NP synthesis, elemental Pt and Pt alloy/intermetallic NPs still suffer from the low utilization of Pt, as the majority of Pt atoms are trapped in the interior of NPs and are not exposed to reactants.

Fabricating core/shell nanostructures with Pt atoms only positioned in a thin shell (<2 nm) is a promising strategy to increase the Pt surface exposure as well as to enhance the Pt activity for ORR through core/shell interaction.[28,29] Herein, we present the synthesis of monodisperse core/shell NPs with a thin FePt shell (≈1 nm) surrounding a Ni core and demonstrate their subsequent conversion to Ni/Pt core/shell NPs. In previous studies of core/shell NPs, one often prepares them by growing Pt or Pt alloy onto non-Pt seeds through seed-mediated growth[30−37] or selective galvanic replacement.[38−40] But the choice of NP seed (core) materials used thus far has always been precious metals such as Au, Pd, and their alloys, as these Au, Pd-related cores have the stable metallic nature and the minimal crystal lattice mismatches with Pt. However, it would be preferable to choose a nonprecious metal, like Ni, Co, or Fe, as the core, ideally Ni which has been proven to be highly effective in balancing the Pt surface energetics in single-crystalline thin film study.[26] Considering the NPs of Ni are subject to rapid surface oxidation, we envisioned that the surface oxidation of these seeds might interfere with the growth of uniform Pt or Pt alloy shell around them. Using the Ni NP seeds protected from oxidation, we obtained monodisperse core/shell Ni/FePt NPs with a thin FePt shell (≈1 nm) (Scheme 1). Conversely, the surface-oxidized Ni seeds led exclusively to the separated FePt NPs. The Ni/FePt NPs were surface activated and transformed to Ni/Pt by acetic acid wash, becoming a highly active catalyst for ORR. The catalytic activity of Ni/Pt was optimized by tuning Ni core size from 4.2 to 9 nm. The specific activity and mass activity of 4.2/0.8 nm core/shell Ni/FePt after acetic acid wash reached 1.95 mA/cm^2 and 490 mA/mg$_{Pt}$ at 0.9 V (vs reversible hydrogen

Scheme 1

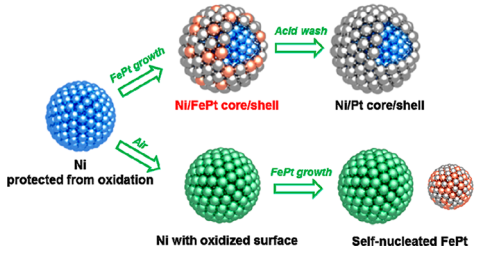

Received: September 25, 2014
Published: October 28, 2014

dx.doi.org/10.1021/ja5099066 | J. Am. Chem. Soc. 2014, 136, 15921−15924

electrode, RHE), while those of benchmark Pt catalyst are only 0.34 mA/cm^2 and 92 mA/mg$_{Pt}$ at 0.9 V.

Ni/FePt NPs were synthesized by the reduction of platinum acetylacetonate (Pt(acac)$_2$) and the thermal decomposition of iron pentacarbonyl (Fe(CO)$_5$) in the presence of Ni NPs (Supporting Information). In the synthesis, the monodisperse Ni NPs were made by modifying a previously reported method.[41] These Ni NPs were stabilized by a surfactant mixture of trioctylphosphine (TOP) (or tributylphosphine (TBP)) and oleylamine which bound to the surface Ni atoms while leaving Ni in its metallic zero-valence state. By changing the choice of surfactants (TOP or TBP) and molar ratio of the Ni precursor (Ni(acac)$_2$)/surfactant, the sizes of Ni NPs were readily tuned to be 4.2 ± 0.2 nm, 7.4 ± 0.3, and 9 ± 0.5 nm, as shown in the transmission electron microscopy (TEM) images (Figure 1A–C). To protect the Ni NPs from oxidation, we synthesized the NPs using Schlenk technique under static N_2 atmosphere and purified the NPs with degassed and dried solvents in N_2-filled glovebox. FePt nucleation and coating were then facilitated by the thermal decomposition of Fe(CO)$_5$, which generated the CO to reduce Pt(II) and atomic Fe to alloy with Pt. Using these size-tunable Ni seeds, the uniform coating of ≈1 nm FePt were achieved, and NP's sizes were increased to 5.8 ± 0.3 nm (4.2 nm Ni), 8.9 ± 0.4 nm (7.4 nm Ni), and 10.6 ± 0.6 nm (9 nm Ni), respectively (Figure 1D–F). The monodisperse Ni/FePt NPs could be produced without any size screening processes and could easily form large-area superlattices due to their highly uniform sizes (Figures S1–3).

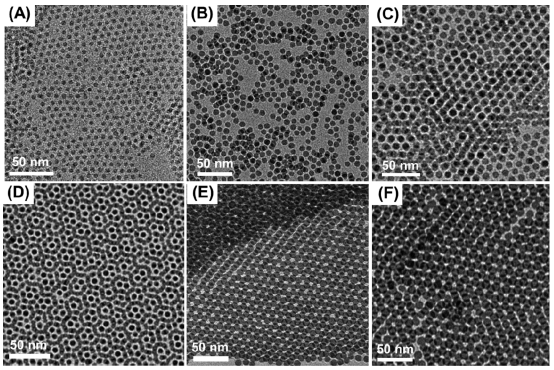

Figure 1. TEM images of the as-synthesized Ni and Ni/FePt core/shell NPs: (A) 4.2 nm Ni, (B) 7.4 nm Ni, (C) 9 nm Ni, (D) 5.8 nm Ni/FePt, (E) 8.9 nm Ni/FePt, and (F) 10.6 nm Ni/FePt. The NP samples in D–F were obtained via the seed-mediated growth by using the NP samples of A–C as seeds, respectively.

The control experiments demonstrated that suppressing the surface oxidation of Ni seeds was crucial for the uniform coating of FePt shell. If the Ni seeds purified under the ambient conditions (surface oxidized) were used as seeds, the product was the mixture of self-nucleated 3–5 nm FePt NPs and Ni NPs which were unchanged in size (Figure S4). The dramatic difference in the NP growth may result from two effects related to Ni's surface oxidation. First, oxidized Ni surface (normally NiO) has a large crystal lattice mismatch with FePt and Pt. Second, the lattice difference and strain between Ni and FePt can be buffered by the alloying of Ni and FePt in the interface which would not be possible with NiO surface.[36] Apart from using the protected Ni seeds, the reaction conditions for FePt coating should also be adjusted to ensure the slow growth of FePt. Specifically, our method of using mixed surfactant of oleylamine and oleic acid is highly efficient in slowing the FePt nucleation/growth[42] and making FePt shell uniform. In contrast, if only oleic acid was used in the reaction, the FePt tended to burst nucleate into separate 3 nm FePt NPs (Figure S5).

X-ray diffraction (XRD) patterns of the Ni and Ni/FePt NPs are shown in Figure 2A. The 4.2 nm Ni NPs show a poor crystallinity with a broadened peak close to (111) peak of face centered cubic (fcc) Ni.[43] The 5.8 nm Ni/FePt based on 4.2 nm Ni also shows weak peak intensity in its XRD pattern and a down-shifted (111) peak located between standard (111) peak positions of fcc-Ni and fcc-FePt, which is similar to previously reported Au/FePt, AgPd/Pt NPs.[31,35] But in the case of 8.9 nm Ni/FePt NPs, the (111) peaks of fcc-Ni and fcc-FePt can be readily distinguished due to the improved crystallinity with larger NP's size, which clearly demonstrates the Ni core is present in the Ni/FePt NPs. The as-prepared Ni/FePt NPs were also characterized with aberration-corrected scanning transmission electron microscopy (STEM) and STEM-electron energy-loss spectroscopy (STEM-EELS). A bright ≈1 nm shell can be visualized in the high-angle annular dark field (HAADF) image of the NPs due to the higher *Z*-contrast of Pt comparing to Ni (Figures 2B and S6).[44] Figures S6 and 2C are the STEM-EELS line scans of the representative 5.8 and 8.9 nm Ni/FePt NPs. It is clearly seen that Ni is located in the core and displays a spherical-like symmetry in 1D elemental distribution, while Pt shows the typical shell-like distribution with a ≈1 nm shell thickness and a plateau over the core region.

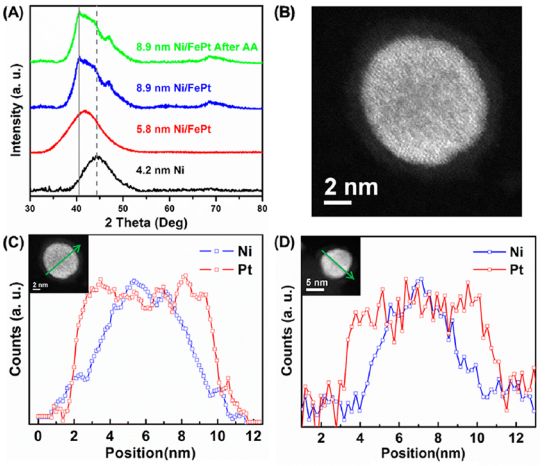

Figure 2. (A) XRD patterns of as-synthesized 4.2 nm Ni, 5.8 nm Ni/FePt, 8.9 nm Ni/FePt supported on C and AA-treated 8.9 nm Ni/FePt supported on C (gray solid line and gray dash line donate the (111) peaks of bulky fcc-FePt and fcc-Ni, respectively). (**B**) HAADF-STEM imaging of a representative as-synthesized 8.9 nm Ni/FePt; (C, D) STEM-EELS line scans crossing the representative as-synthesized 8.9 nm Ni/FePt (C) and AA-treated 8.9 nm Ni/FePt supported on C (D). The insets show the NPs scanned.

Inductively coupled plasma-optical emission spectroscopy was used to characterize the compositions of the as-prepared Ni/FePt NPs. The 5.8, 8.9, and 10.6 nm Ni/FePt NPs show the atomic compositions of $Ni_{41}Pt_{42}Fe_{17}$, $Ni_{35}Pt_{47}Fe_{18}$, and $Ni_{29}Pt_{55}Fe_{16}$, respectively, suggesting more Pt was needed to grow ≈1 nm shell on larger Ni seeds (Table S1). Along with the formation of FePt shells, the surfactant bound to NPs also changed. The Ni NPs were surrounded by a large amount of TBP/TOP (Ni:P = 70:30 in 4.2 nm Ni), as indicated by energy-dispersive X-ray spectroscopy (EDS) spectrum in Figure S7. But

dx.doi.org/10.1021/ja5099066 | J. Am. Chem. Soc. 2014, 136, 15921–15924

after coating with FePt, the P signal was undetectable in the EELS spectrum (Figure S8) (P Kα and Pt M peaks overlap in EDS). Clearly, the as-synthesized Ni/FePt NPs were stabilized by OAm/OAc.

To remove the surfactants of OAm/OAc surrounding NPs, the Ni/FePt NPs were deposited on Ketjen carbon (C) support (denoted as C-NPs) and then treated with glacial acetic acid (AA) at 70 °C for 24 h (Supporting Information). This approach has been widely used to remove the hydrophobic OAm/OAc from other Pt-based NPs.[32] Figure S9 shows the typical TEM images of the Ni/FePt NPs before and after the AA wash. NP morphology is maintained after the AA wash, indicating the Ni core is stabilized by the uniform Pt-rich shell. The preservation of Ni core after AA treatment was also validated by the XRD pattern of AA-treated 8.9 nm NPs supported on C (Figure 2A). Correspondingly, the Ni/Pt atomic ratio was only slightly decreased in all Ni/FePt NPs after AA treatment (Table S1). But the most of Fe located in the shell was lost, making Fe atomic content in FePt <5% in the AA-treated NPs (we still use the Ni/FePt in the following description for consistency). We also characterized the AA-treated C-NPs by using STEM. STEM-EELS line scan on the AA-treated 5.8 and 8.9 nm NPs further confirmed the Ni/Pt core/shell structures in both NP samples (Figures 2D and S10).

The AA-treated C-NPs and commercial Pt catalyst (2.5−3.5 nm Pt particles on C, Fuel Cells Store, denoted as Comm-Pt) were dispersed in the mixture of isopropanol and water containing Nafion under sonication. The catalyst ink was transferred onto a glassy carbon surface of the rotating disk electrode, forming an electrode decorated by a thin film of catalyst for electrochemical testing. Figure S11 shows the cyclic voltammograms of Comm-Pt and three different sizes of Ni/FePt NPs with the similar Pt weight loading in the N_2-saturated 0.1 M $HClO_4$. All the catalysts showed the typical hydrogen underpotential formation/stripping peaks (H_{UPD}) in the potential range of 0.05−0.35 V (vs RHE), the integral areas of which were used to estimate the electrochemically active surface areas (ECASA) of the catalysts.[45] With the similar Pt weight loading, smaller NP yielded larger ECASA. The catalysts also exhibited Pt metal oxidation/reduction peaks in the potential range of 0.5−1.06 V (vs RHE).

The Ni/FePt NPs with the different core sizes and the same shell thickness were studied for ORR catalysis. Figure 3A shows the ORR polarization curves of the Ni/FePt core/shell NPs and Comm-Pt NPs in O_2-saturated 0.1 M $HClO_4$ with the electrode rotation rate of 1600 rpm. Each curve contains the diffusion-limiting current region from 0.3 to ∼0.65 V and the mixed kinetic−diffusion control region from ∼0.65 to ∼1 V. All the Ni/FePt NPs show the ORR curves positively shifted relative to Comm-Pt, indicating the Ni/FePt NPs have the higher activities than Comm-Pt. The best half-wave potential ($E_{1/2}$) occurs in 5.8 nm Ni/FePt (0.913 V), higher than that of 8.9 nm Ni/FePt (0.901 V), 10.6 nm Ni/FePt (0.888 V), and Comm-Pt catalyst (0.865 V). The specific and mass activities of the catalysts were extracted by normalizing their ORR kinetic current densities over ECASA and Pt mass, respectively. At 0.9 V (vs RHE), three sizes of the Ni/FePt NPs exhibited similar specific activities in the range of 1.95−2.18 mA/cm^2, while the Comm-Pt had a specific activity of only 0.34 mA/cm^2 (Figure 3B). This indicates that Pt's inherent surface activity is dramatically enhanced due to the core/shell structure. According to the previous theoretical and experimental reports, the Pt surface energetics can be tuned by the core when the Pt shell is very thin (<2 nm).[32,46,47] Since the

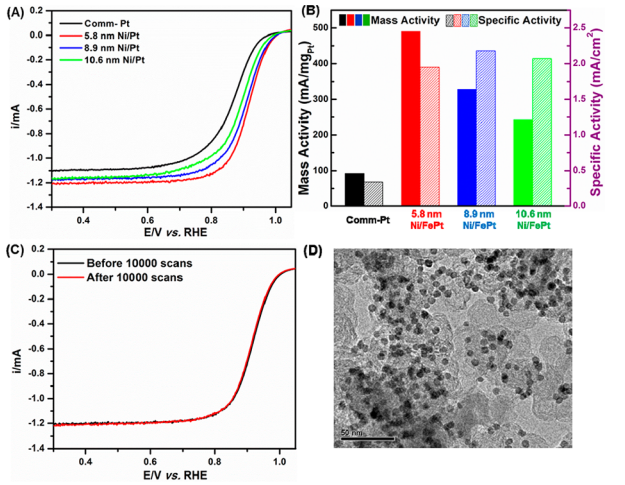

Figure 3. (A) ORR polarization curves of the Comm-Pt and 5.8, 8.9, and 10.6 nm Ni/FePt catalysts. (B) The mass and specific activities of the Comm-Pt and 5.8, 8.9, and 10.6 nm Ni/FePt catalysts at 0.9 V (vs RHE). (C) ORR polarization curves of the 5.8 nm Ni/FePt catalyst before and after stability test of 10,000 potential scans. (D) TEM image of the 5.8 nm Ni/FePt catalyst after stability test of 10,000 potential scans.

Ni is one of the most effective metals to optimize the Pt d-band center through electronic and strain effects,[18,26] the ≈1 nm Pt shell supported by Ni core becomes highly active in catalyzing ORR. Ni/FePt NPs exhibited core size-dependent mass activities at 0.9 V in the order of 5.8 nm (490 mA/mg$_{Pt}$) > 8.9 nm (328 mA/mg$_{Pt}$) > 10.6 nm (242 mA/mg$_{Pt}$), which was consistent with the ECASA trend of the Ni/FePt NPs (Figure 3B). All the Ni/FePt NP catalysts had mass activities higher than Comm-Pt at 0.9 V (92 mA/mg$_{Pt}$) with the 5.8 nm one exceeding the 2017 U.S. Department of Energy target for an ORR catalyst (440 mA/mg$_{Pt}$).

We also investigated the catalytic stability of Ni/FePt NPs by cycling them in the potential range of 0.66 to 1.06 V (vs RHE) in the O_2-saturated 0.1 M $HClO_4$. After 10,000 sweeps, we observed no change in 5.8 nm NP morphology (Figure 3D) and only a slight decrease in Ni composition (from $Ni_{46}Pt_{54}$ to $Ni_{37}Pt_{63}$). This provides further evidence that the uniform ≈1 nm Pt shell can protect the Ni core. Moreover, no obvious shift in ORR polarization curve was found after stability test on 5.8 nm Ni/FePt, suggesting the Ni/FePt NPs were highly stable under the ORR condition (Figure 3C).

We present the synthesis of monodisperse Ni/FePt and their conversion to Ni/Pt core/shell NPs with high catalytic activity and durability for ORR. The core/shell Ni/FePt NPs were synthesized by a solution-phase seed-mediated growth where the FePt shell thickness was ∼1 nm and the core size was tuned from 4.2 to 9 nm. Carefully minimizing surface oxidation of Ni seeds was crucial for the core/shell formation; only Ni protected from oxidation led to uniform FePt coating. The Ni/FePt NPs were converted to Ni/Pt after AA wash, resulting in an active catalyst for ORR. Their ORR catalytic efficiency could be further improved by tuning NP's core size. The 5.8 nm Ni/FePt after AA wash was a highly active and durable catalyst with the specific activity and mass activity reaching 1.95 mA/cm^2 and 490 mA/mg$_{Pt}$ at 0.9 V, whereas the benchmark commercial Pt catalyst showed only 0.34 mA/cm^2 and 92 mA/mg$_{Pt}$. The work highlights the great potential of core/shell NPs as highly efficient catalysts for ORR, which could be further generalized for many other heterogeneous catalytic reactions.

dx.doi.org/10.1021/ja5099066 | J. Am. Chem. Soc. 2014, 136, 15921−15924

■ ASSOCIATED CONTENT

Supporting Information

Materials, Ni and Ni/FePt nanoparticle synthesis and characterizations, and their electrochemical measurements; Table S1; Figures S1−S11. This material is available free of charge via the Internet at http://pubs.acs.org.

■ AUTHOR INFORMATION

Corresponding Author

cbmurray@sas.upenn.edu

Notes

The authors declare no competing financial interest.

■ ACKNOWLEDGMENTS

This work was supported by NatureNet Science Fellowship from The Nature Conservancy. Partial work on electron microscopy carried out at the Center for Functional Nanomaterials, Brookhaven National Laboratory, was supported by the U.S. Department of Energy, Office of Basic Energy Sciences, under contract no. DE-AC02-98CH10886. Partial work on Ni nanoparticle chemistry was supported by the Catalysis Center for Energy Innovation, an Energy Frontier Research Center funded by the U.S. Department of Energy, Office of Science, Office of Basic Energy Sciences under award no. DE-SC0001004. Partial work on electrochemistry was supported by the U.S. Department of Energy, Office of Energy Efficiency and Renewable Energy, Fuel Cell Technologies Program and by the U.S. Army Research Laboratory and the U.S. Army Research Office under the Multi University Research Initiative (MURI, grant no. W911NF-11-1-0353) on "Stress-Controlled Catalysis via Engineered Nanostructures".

■ REFERENCES

(1) Stamenkovic, V. R.; Fowler, B.; Mun, B. S.; Wang, G.; Ross, P. N.; Lucas, C. A.; Markovic, N. M. *Science* **2007**, *315*, 493−497.

(2) Guo, S.; Zhang, S.; Sun, S. *Angew. Chem., Int. Ed.* **2013**, *52*, 8526−8554.

(3) Wang, C.; Markovic, N. M.; Stamenkovic, V. R. *ACS Catal.* **2012**, *2*, 891−898.

(4) Wu, J.; Yang, H. *Acc. Chem. Res.* **2013**, *46*, 1848−1857.

(5) Li, H.-H.; Cui, C.-H.; Zhao, S.; Yao, H.-B.; Fan, F.-J.; Yu, S.-H. *Adv. Energy Mater.* **2012**, *2*, 1182−1187.

(6) Cui, C.-H.; Yu, S.-H. *Acc. Chem. Res.* **2013**, *46*, 1427−1437.

(7) Wang, C.; Vliet, van der D.; Chang, K.-C.; You, H.; Strmcnik, D.; Schlueter, J. A.; Markovic, N. M.; Stamenkovic, V. R. *J. Phys. Chem. C* **2009**, *113*, 19365−19368.

(8) Wang, C.; Daimon, H.; Onodera, T.; Koda, T.; Sun, S. *Angew. Chem., Int. Ed.* **2008**, *47*, 3588−3591.

(9) Cui, C.-H.; Gan, L.; Heggen, M.; Rudi, S.; Strasser, P. *Nat. Mater.* **2013**, *12*, 765−771.

(10) Chen, C.; Kang, Y.; Huo, Z.; Zhu, Z.; Huang, W.; Xin, H.; Snyder, J. D.; Li, D.; Herron, J. A.; Mavrikakis, M.; Chi, M.; More, K. L.; Li, Y.; Markovic, N. M.; Somorjai, G. A.; Yang, P.; Stamenkovic, V. R. *Science* **2014**, *343*, 1339−1343.

(11) Zhang, J.; Yang, H.; Fang, J.; Zou, S. *Nano Lett.* **2010**, *10*, 638−644.

(12) Choi, S.-I.; Xie, S.; Shao, M.; Odell, J. H.; Lu, N.; Peng, H.-C.; Protsailo, L.; Guerrero, S.; Park, J.; Xia, X.; Wang, J.; Kim, M. J.; Xia, Y. *Nano Lett.* **2013**, *13*, 3420−3425.

(13) Wu, J.; Qi, L.; You, H.; Gross, A.; Li, J.; Yang, H. *J. Am. Chem. Soc.* **2012**, *134*, 11880−11883.

(14) Guo, S.; Li, D.; Zhu, H.; Zhang, S.; Markovic, N. M.; Stamenkovic, V. R.; Sun, S. *Angew. Chem., Int. Ed.* **2013**, *52*, 3465−3468.

(15) Kang, Y.; Murray, C. B. *J. Am. Chem. Soc.* **2010**, *132*, 7568−7569.

(16) Cui, C.-H.; Gan, L.; Neumann, M.; Heggen, M.; Cuenya, B. R.; Strasser, P. *J. Am. Chem. Soc.* **2014**, *136*, 4813−4816.

(17) Wang, C.; Chi, M.; Li, D.; Vliet, van der D.; Wang, G.; Lin, Q.; Mitchell, J. F.; More, K. L.; Markovic, N. M.; Stamenkovic, V. R. *ACS Catal.* **2011**, *1*, 1355−1359.

(18) Zhu, H.; Zhang, S.; Guo, S.; Su, D.; Sun, S. *J. Am. Chem. Soc.* **2013**, *135*, 7130−7133.

(19) Cui, C.-H.; Li, H.-H.; Yu, J.-W.; Gao, M.-R.; Yu, S.-H. *Angew. Chem., Int. Ed.* **2010**, *49*, 9149−9152.

(20) Li, H.-H.; Zhao, S.; Gong, M.; Cui, C.-H.; He, D.; Liang, H.-W.; Wu, L.; Yu, S.-H. *Angew. Chem., Int. Ed.* **2013**, *52*, 7472−7476.

(21) Zhang, S.; Zhang, X.; Jiang, G.; Zhu, H.; Guo, S.; Su, D.; Lu, G.; Sun, S. *J. Am. Chem. Soc.* **2014**, *136*, 7734−7739.

(22) Wang, D.; Xin, H. L.; Hovden, R.; Wang, H.; Yu, Y.; Muller, D. A.; DiSalvo, F. J.; Abruña, H. D. *Nat. Mater.* **2013**, *12*, 81−87.

(23) Chen, H.; Wang, D.; Yu, Y.; Newton, K. A.; Muller, D. A.; Abruña, H. D.; DiSalvo, F. J. *J. Am. Chem. Soc.* **2012**, *134*, 18453−18459.

(24) Zhang, S.; Guo, S.; Zhu, H.; Su, D.; Sun, S. *J. Am. Chem. Soc.* **2012**, *134*, 5060−5063.

(25) Prabhudev, S.; Bugnet, M.; Bock, C.; Botton, G. A. *ACS Nano* **2013**, *7*, 6103−6110.

(26) Stamenkovic, V. R.; Mun, B. S.; Arenz, M.; Mayrhofer, K. J. J.; Lucas, C. A.; Wang, G.; Ross, P. N.; Markovic, N. M. *Nat. Mater.* **2007**, *6*, 241−247.

(27) Strasser, P.; Koh, S.; Anniyev, T.; Greeley, J.; More, K. L.; Yu, C.; Liu, Z.; Kaya, S.; Nordlund, D.; Ogasawara, H.; Toney, M. F.; Nilsson, A. *Nat. Chem.* **2010**, *2*, 454−460.

(28) Adzic, R. R.; Zhang, J.; Sasaki, K.; Vukmirovic, M. B.; Shao, M.; Wang, J. X.; Nilekar, A. U.; Mavrikakis, M.; Uribe, F. *Top. Catal.* **2007**, *46*, 249−262.

(29) Yang, H. *Angew. Chem., Int. Ed.* **2011**, *50*, 2674−2676.

(30) Lim, B.; Jiang, M.; Camargo, P. H. C.; Cho, E. C.; Tao, J.; Lu, X.; Zhu, Y.; Xia, Y. *Science* **2009**, *324*, 1302−1305.

(31) Wang, C.; Vliet, D.; More, K.; Zaluzec, N.; Peng, S.; Sun, S.; Daimon, H.; Wang, G.; Greeley, J.; Pearson, J.; Paulikas, A.; Karapetrov, G.; Strmcnik, D.; Markovic, N. M.; Stamenkovic, V. R. *Nano Lett.* **2011**, *11*, 919−926.

(32) Mazumder, V.; Chi, M.; More, K. L.; Sun, S. *J. Am. Chem. Soc.* **2010**, *5*, 7848−7849.

(33) Sun, X.; Li, D.; Ding, Y.; Zhu, W.; Guo, S.; Wang, Z. L.; Sun, S. *J. Am. Chem. Soc.* **2014**, *136*, 5745−5749.

(34) Yang, J.; Chen, X.; Yang, X.; Ying, J. Y. *Energy Environ. Sci.* **2012**, *5*, 8976−8981.

(35) Yang, J.; Yang, J.; Ying, J. Y. *ACS Nano* **2012**, *6*, 9373−9382.

(36) Ysieh, Y.-C.; Zhang, Y.; Su, D.; Volkov, V.; Si, R.; Wu, L.; Zhu, Y.; An, W.; Liu, P.; He, P.; Ye, S.; Adzic, R. R.; Wang, J. X. *Nat. Commun.* **2013**, *4*, 2466−2464.

(37) Guo, S.; Zhang, S.; Su, D.; Sun, S. *J. Am. Chem. Soc.* **2013**, *135*, 13879−13884.

(38) Zhang, J.; Mo, Y.; Vukmirovic, M. B.; Klie, R.; Sasaki, K.; Adzic, R. R. *J. Phys. Chem. B* **2004**, *108*, 10955−10964.

(39) Gong, K.; Su, D.; Adzic, R. R. *J. Am. Chem. Soc.* **2010**, *132*, 14364−14366.

(40) Sasaki, K.; Naohara, H.; Choi, Y.; Cai, Y.; Chen, W.-F.; Liu, P.; Adzic, R. R. *Nat. Commun.* **2012**, *3*, 1115−1123.

(41) Cargnello, M.; Doan-Nguyen, V. V. T.; Gordon, T. R.; Diaz, R. E.; Stach, E. A.; Gorte, R. J.; Fornasiero, P.; Murray, C. B. *Science* **2013**, *341*, 771−773.

(42) Kim, J.; Rong, C.; Liu, J. P.; Sun, S. *Adv. Mater.* **2009**, *21*, 906−909.

(43) Doan-Nguyen, V. V. T.; Kimber, S. A. J.; Pontoni, D.; Hickey, D. R.; Diroll, B. T.; Yang, X.; Miglierini, M.; Murray, C. B.; Billinge, S. J. L. *ACS Nano* **2014**, *8*, 6163−6170.

(44) Pennycook, S. J. *Ultramicroscopy* **1989**, *30*, 58−69.

(45) Snyder, J.; Fujita, T.; Chen, M. W.; Erlebacher, J. *Nat. Mater.* **2010**, *9*, 904−907.

(46) Zhang, X.; Lu, G. *J. Phys. Chem. Lett.* **2014**, *5*, 292−297.

(47) Shao, M.; Odell, J. H.; Peles, A.; Su, D. *Chem. Commun.* **2014**, *50*, 2173−2176.